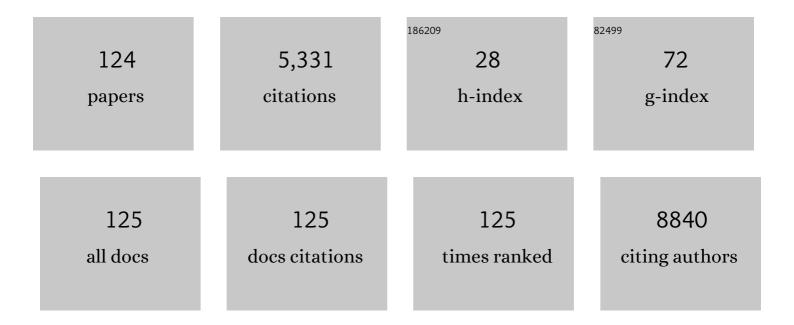
## **Cheol-Woong Yang**

List of Publications by Year in descending order

Source: https://exaly.com/author-pdf/7408450/publications.pdf Version: 2024-02-01



#	Article	IF	CITATIONS
1	Evidence of Graphitic AB Stacking Order of Graphite Oxides. Journal of the American Chemical Society, 2008, 130, 1362-1366.	6.6	995
2	Wafer-Scale Growth of Single-Crystal Monolayer Graphene on Reusable Hydrogen-Terminated Germanium. Science, 2014, 344, 286-289.	6.0	831
3	Synthesis of Largeâ€Area Graphene Layers on Polyâ€Nickel Substrate by Chemical Vapor Deposition: Wrinkle Formation. Advanced Materials, 2009, 21, 2328-2333.	11.1	814
4	Dirac electrons in a dodecagonal graphene quasicrystal. Science, 2018, 361, 782-786.	6.0	223
5	Synthesis of Silicon Nanotubes on Porous Alumina Using Molecular Beam Epitaxy. Advanced Materials, 2003, 15, 1172-1176.	11.1	165
6	X-ray photoemission spectroscopy study of fluorinated single-walled carbon nanotubes. Applied Physics Letters, 2002, 80, 4235-4237.	1.5	153
7	Role of Anions in the AuCl <sub>3</sub> -Doping of Carbon Nanotubes. ACS Nano, 2011, 5, 1236-1242.	7.3	149
8	Intermetallic compound layer growth at the interface between Sn–Cu–Ni solder and Cu substrate. Journal of Alloys and Compounds, 2004, 381, 151-157.	2.8	99
9	Large-scale production of aligned carbon nanotubes by the vapor phase growth method. Chemical Physics Letters, 2002, 359, 109-114.	1.2	89
10	Design of Dispersants for the Dispersion of Carbon Nanotubes in an Organic Solvent. Advanced Functional Materials, 2007, 17, 1775-1783.	7.8	87
11	Single-walled carbon nanotubes produced by catalytic chemical vapor deposition of acetylene over Fe–Mo/MgO catalyst. Chemical Physics Letters, 2004, 383, 104-108.	1.2	82
12	One-pot synthesis of core–shell-like Pt3Co nanoparticle electrocatalyst with Pt-enriched surface for oxygen reduction reaction in fuel cells. Energy and Environmental Science, 2011, 4, 4947.	15.6	81
13	High-Quality Double-Walled Carbon Nanotubes Produced by Catalytic Decomposition of Benzene. Chemistry of Materials, 2003, 15, 3951-3954.	3.2	78
14	Electrically Driven Reversible Phase Changes in Layered In <sub>2</sub> Se <sub>3</sub> Crystalline Film. Advanced Materials, 2017, 29, 1703568.	11.1	77
15	High-Yield Catalytic Synthesis of Thin Multiwalled Carbon Nanotubes. Journal of Physical Chemistry B, 2004, 108, 17695-17698.	1.2	71
16	Dispersion Stability of Single-Walled Carbon Nanotubes Using Nafion in Bisolvent. Journal of Physical Chemistry C, 2007, 111, 2477-2483.	1.5	66
17	Detection of graphene domains and defects using liquid crystals. Nature Communications, 2014, 5, 3484.	5.8	62
18	Large-Scale Synthesis of High-Quality Double-Walled Carbon Nanotubes by Catalytic Decomposition of n-Hexane, Journal of Physical Chemistry B, 2004, 108, 2192-2194	1.2	60

#	Article	IF	CITATIONS
19	Synthesis of single- and double-walled carbon nanotubes by catalytic decomposition of methane. Chemical Physics Letters, 2003, 373, 475-479.	1.2	57
20	Epitaxial-Growth-Induced Junction Welding of Silver Nanowire Network Electrodes. ACS Nano, 2018, 12, 4894-4902.	7.3	56
21	Epitaxial Growth of a Single-Crystal Hybridized Boron Nitride and Graphene Layer on a Wide-Band Gap Semiconductor. Journal of the American Chemical Society, 2015, 137, 6897-6905.	6.6	55
22	Waferâ€Scale and Lowâ€Temperature Growth of 1Tâ€WS <sub>2</sub> Film for Efficient and Stable Hydrogen Evolution Reaction. Small, 2020, 16, e1905000.	5.2	53
23	Effects of deposition parameters on the crystallinity of CeO2 thin films deposited on Si(100) substrates by r.fmagnetron sputtering. Thin Solid Films, 2000, 360, 154-158.	0.8	52
24	Quantum Confinement Effects in Transferrable Silicon Nanomembranes and Their Applications on Unusual Substrates. Nano Letters, 2013, 13, 5600-5607.	4.5	49
25	Realization of continuous Zachariasen carbon monolayer. Science Advances, 2017, 3, e1601821.	4.7	46
26	Low-temperature wafer-scale growth of MoS2-graphene heterostructures. Applied Surface Science, 2019, 470, 129-134.	3.1	44
27	Title is missing!. Journal of Materials Science: Materials in Electronics, 2003, 14, 487-493.	1.1	41
28	Thickness contrast of fewâ€layered graphene in SEM. Surface and Interface Analysis, 2012, 44, 1538-1541.	0.8	35
29	Control of interfacial reaction layers formed in Sn–3.5Ag–0.7Cu/electroless Ni–P solder joints. Scripta Materialia, 2009, 60, 257-260.	2.6	27
30	Study of ZrO2 thin films for gate oxide applications. Journal of Vacuum Science and Technology A: Vacuum, Surfaces and Films, 2001, 19, 1720-1724.	0.9	25
31	Characteristics of HfO[sub 2]/HfSi[sub x]O[sub y] film as an alternative gate dielectric in metal–oxide–semiconductor devices. Journal of Vacuum Science & Technology an Official Journal of the American Vacuum Society B, Microelectronics Processing and Phenomena, 2002, 20, 1360.	1.6	25
32	Formation of Reliable HfO2/HfSixOyGate-Dielectric for Metal-Oxide-Semiconductor Devices. Japanese Journal of Applied Physics, 2002, 41, 6904-6907.	0.8	25
33	High-Temperature Chemical Vapor Deposition for SiC Single Crystal Bulk Growth Using Tetramethylsilane as a Precursor. Crystal Growth and Design, 2014, 14, 5569-5574.	1.4	25
34	Active-matrix monolithic gas sensor array based on MoS2 thin-film transistors. Communications Materials, 2020, 1, .	2.9	25
35	Characterization of ternary Ni2SnP layer in Sn–3.5Ag–0.7Cu/electroless Ni (P) solder joint. Scripta Materialia, 2010, 63, 1108-1111.	2.6	24
36	Characterization of Interfacial Reaction Layers Formed Between Sn-3.5Ag Solder and Electroless Ni-Immersion Au-Plated Cu Substrates. Journal of Electronic Materials, 2008, 37, 84-89.	1.0	22

#	Article	IF	CITATIONS
37	Microstructural Characterization of SS304 upon Various Shot Peening Treatments. Applied Microscopy, 2015, 45, 155-169.	0.8	22
38	Characteristics of an Amorphous Carbon Layer as a Diffusion Barrier for an Advanced Copper Interconnect. ACS Applied Materials & Interfaces, 2020, 12, 3104-3113.	4.0	21
39	Electroplated Silver–Nickel Core–Shell Nanowire Network Electrodes for Highly Efficient Perovskite Nanoparticle Light-Emitting Diodes. ACS Applied Materials & Interfaces, 2020, 12, 39479-39486.	4.0	21
40	Surface Nanocrystallization of Pure Cu Induced by Ultrasonic Shot Peening. Journal of Nanoscience and Nanotechnology, 2014, 14, 9637-9643.	0.9	18
41	Crystallographic alignment of Fe2B and Nd2Fe14B for texture memory in hydrogenation–disproportionation–desorption–recombination-processed Nd–Fe–B powders. Journal of Alloys and Compounds, 2018, 732, 32-42.	2.8	16
42	MORPHOLOGY, THERMAL STABILITY, AND SOLDERABILITY OF ELECTROLESS NICKEL–PHOSPHORUS PLATING LAYER. Surface Review and Letters, 2007, 14, 827-832.	0.5	15
43	Investigation of Zirconium Effect on the Corrosion Resistance of Aluminum Alloy Using Electrochemical Methods and Numerical Simulation in an Acidified Synthetic Sea Salt Solution. Materials, 2018, 11, 1982.	1.3	15
44	Effect of buffer layer on the growth of GaN on Si substrate. Journal of Crystal Growth, 2002, 237-239, 1094-1098.	0.7	14
45	Initial interfacial reaction layers formed in Sn–3.5Ag solder/electroless Ni–P plated Cu substrate system. Journal of Materials Research, 2008, 23, 2195-2201.	1.2	14
46	In situ TEM characterization of interfacial reaction in Sn–3.5Ag/electroless Ni(P) solder joint. Scripta Materialia, 2011, 64, 597-600.	2.6	14
47	Improvement of corrosion penetration resistance for aluminum heat exchanger by alloying zirconium. Materials Chemistry and Physics, 2020, 241, 122275.	2.0	12
48	The effects of Ta on the formation of Ni-silicide in Ni0.95xTax0.05/Si systems. Materials Science and Engineering B: Solid-State Materials for Advanced Technology, 2004, 114-115, 241-245.	1.7	11
49	Effect of the dehydrogenation speed and Nd content on the microstructure and magnetic properties of HDDR processed Nd-Fe-B magnets. Metals and Materials International, 2014, 20, 909-914.	1.8	11
50	Effect of Ultrasonic Nanocrytalline Surface Modification on the Microstructural Evolution of Inconel 690 Alloy. Materials and Manufacturing Processes, 2015, 30, 194-198.	2.7	10
51	Superconducting joint between Bi-Pb-Sr-Ca-Cu-O superconductor tapes. IEEE Transactions on Applied Superconductivity, 2000, 10, 1182-1185.	1.1	9
52	Core–shell Si <sub>1â^'x</sub> Ge <sub>x</sub> nanowires with controlled structural defects for phonon scattering enhancement. Journal of Materials Chemistry A, 2014, 2, 12153-12157.	5.2	9
53	Direct observation of texture memory in hydrogenation–disproportionation–desorption–recombination processed Nd-Fe-B magnets using electron backscatter diffraction. Scripta Materialia, 2016, 115, 6-9.	2.6	9
54	Temperature Calibration of a Specimen-heating Holder for Transmission Electron Microscopy. Applied Microscopy, 2015, 45, 95-100.	0.8	9

#	Article	IF	CITATIONS
55	Dynamic study on microstructural evolution of nickel germanide utilizing zirconium interlayer. Microelectronic Engineering, 2012, 89, 23-26.	1.1	8
56	Formation of an oxygen vacancy-dinitrogen complex in nitrogen-doped hafnium oxide. Journal of Analytical Atomic Spectrometry, 2013, 28, 482.	1.6	8
57	Amorphous TaxMnyOz Layer as a Diffusion Barrier for Advanced Copper Interconnects. Scientific Reports, 2019, 9, 20132.	1.6	8
58	Determination of Dy substitution site in Nd2â^'xDyxFe14B by HAADF-STEM and illustration of magnetic anisotropy of "g―and "f―sites, before and after substitution. Scientific Reports, 2021, 11, 6347.	1.6	8
59	Transmission Electron Microscopy Specimen Preparation of Delicate Materials Using Tripod Polisher. Applied Microscopy, 2016, 46, 110-115.	0.8	8
60	Characteristics of ZrO[sub 2] Films with Al and Pt Gate Electrodes. Journal of the Electrochemical Society, 2003, 150, G849.	1.3	7
61	Oxidation Mechanism of Nickel Oxide/Carbon Nanotube Composite. Microscopy and Microanalysis, 2013, 19, 202-206.	0.2	7
62	Residual Hydrogen in Nd-Fe-B HDDR Powder and Its Effect on Coercivity of Hot-Pressed Compact. IEEE Transactions on Magnetics, 2013, 49, 3398-3401.	1.2	7
63	Direct observation of interfacial reaction of Ni/6H-SiC and carbon redistribution by in situ transmission electron microscopy. Materials Characterization, 2018, 140, 259-264.	1.9	7
64	Evaluation of ion/electron beam induced deposition for electrical connection using a modern focused ion beam system. Applied Microscopy, 2019, 49, 6.	0.8	7
65	Work Function Shift Mechanism of Metal-Gate Electrode with Ruâ^•Ti Bilayer. Electrochemical and Solid-State Letters, 2007, 10, H63.	2.2	6
66	Self-assembled Cu(In,Ga)Se2 nanocrystals formed by Ar ion beam irradiation. Solar Energy Materials and Solar Cells, 2012, 105, 119-124.	3.0	6
67	Quantification of crystallinity using zeroâ€loss filtered electron diffraction. Microscopy Research and Technique, 2019, 82, 39-46.	1.2	6
68	Rapid and mass-producible synthesis of high-crystallinity MoSe <sub>2</sub> nanosheets by ampoule-loaded chemical vapor deposition. Nanoscale, 2020, 12, 6991-6999.	2.8	6
69	Surface Nanocrystallization of Pure Ni Induced by Ultrasonic Shot Peening. Science of Advanced Materials, 2017, 9, 188-192.	0.1	6
70	Development of High-Temperature Solders: Contribution of Transmission Electron Microscopy. Applied Microscopy, 2015, 45, 89-94.	0.8	6
71	Microstructure of interfacial reaction layer in Sn–Ag–Cu/electroless Ni (P) solder joint. Journal of Materials Science: Materials in Electronics, 2011, 22, 1308-1312.	1.1	5
72	<i>Inâ€situ</i> observation of ion beamâ€induced nanostructure formation on a Cu(In,Ga)Se <sub>2</sub> Surface. Surface and Interface Analysis, 2012, 44, 1542-1546.	0.8	5

#	Article	IF	CITATIONS
73	Effect of desorption and recombination on texture development in hydrogenation–disproportionation–desorption–recombination processed Nd–Fe–B magnets. Journal of Alloys and Compounds, 2016, 672, 582-589.	2.8	5
74	Novel Method for Preparing Transmission Electron Microscopy Samples of Micrometer-Sized Powder Particles by Using Focused Ion Beam. Microscopy and Microanalysis, 2017, 23, 1055-1060.	0.2	5
75	Effect of Electromigration-Induced Joule Heating on the Reliability of Sn-Ag Microbump with Different UBM Structures. Journal of Electronic Materials, 2020, 49, 7228-7237.	1.0	5
76	Study of the Microstructural Evolution of Tempered Martensite Ferritic Steel T91 upon Ultrasonic Nanocrystalline Surface Modification. Applied Microscopy, 2015, 45, 170-176.	0.8	5
77	Properties of resistive- and superconducting-joints in Bi-Pb-Sr-Ca-Cu-O tape. IEEE Transactions on Applied Superconductivity, 2001, 11, 3010-3013.	1.1	4
78	High Thermal Stability of Ni Monosilicide from Ni-Ta Alloy Films on Si(100). Electrochemical and Solid-State Letters, 2003, 6, G122.	2.2	4
79	Enhanced Morphological and Thermal Stabilities of Nickel Germanide with an Ultrathin Tantalum Layer Studied by Ex Situ and In Situ Transmission Electron Microscopy. Microscopy and Microanalysis, 2013, 19, 114-118.	0.2	4
80	Interfacial Reactions in Ni/6H-SiC at Low Temperatures. Journal of Nanoscience and Nanotechnology, 2016, 16, 10853-10857.	0.9	4
81	Low angle boundary migration of shotâ€peened pure nickel investigated by electron channeling contrast imaging and electron backscatter diffraction. Microscopy Research and Technique, 2019, 82, 849-855.	1.2	4
82	Improvements in Thermal Stability of Sb <sub>2</sub> Te <sub>3</sub> by Modulation of Microstructure via Carbon Incorporation. ACS Applied Electronic Materials, 2021, 3, 3472-3481.	2.0	4
83	Kinetics of the Ni/Ta-Interlayer/Ge Reactions Studied by <i>In Situ</i> Transmission Electron Microscopy. Science of Advanced Materials, 2015, 7, 1497-1501.	0.1	4
84	Effect of (La, Sr)CoO3 seed layer on the reliability of Pb(Zr, Ti)O3 capacitors. Integrated Ferroelectrics, 1999, 25, 341-350.	0.3	3
85	Nickel Doping on Cobalt Oxide Thin Film Using by Sputtering Process-a Route for Surface Modification for p-type Metal Oxide Gas Sensors. Journal of the Korean Physical Society, 2018, 73, 1867-1872.	0.3	3
86	Physical and electrical degradation of ZrO2 thin films with aluminum electrodes. Materials Science and Engineering B: Solid-State Materials for Advanced Technology, 2003, 102, 108-112.	1.7	2
87	TEM study on the interfacial reaction between electroless plated Niâ^P/Au UBM and Snâ^3.5Ag solder. Metals and Materials International, 2007, 13, 235-238.	1.8	2
88	Microstructural evolution of nickel-germanide in the Ni1â^'xTax/Ge systems during in situ annealing. Journal of Vacuum Science and Technology A: Vacuum, Surfaces and Films, 2008, 26, 688-691.	0.9	2
89	Crystallization Behaviour of Electroless Ni-P UBM with Medium Phosphorous Induced by Single and Step Heat Treatment. Materials Transactions, 2010, 51, 1878-1882.	0.4	2
90	Graphene Growth at the Interface Between Ni Catalyst Layer and SiO <sub>2</sub> /Si Substrate. Journal of Nanoscience and Nanotechnology, 2011, 11, 6468-6471.	0.9	2

#	Article	IF	CITATIONS
91	Rehybridization-induced defect-level of open-core edge dislocation in GaN. Scripta Materialia, 2013, 69, 537-540.	2.6	2
92	High-Density Ordered Arrays of CoPt3 Nanoparticles with Individually Addressable Out-of-Plane Magnetization. ACS Applied Nano Materials, 2019, 2, 975-982.	2.4	2
93	Hydrogen Evolution Reaction: Waferâ€Scale and Lowâ€Temperature Growth of 1Tâ€WS <sub>2</sub> Film for Efficient and Stable Hydrogen Evolution Reaction (Small 6/2020). Small, 2020, 16, 2070033.	5.2	2
94	Optimal Conditions for Defect Analysis Using Electron Channeling Contrast Imaging. Applied Microscopy, 2016, 46, 164-166.	0.8	2
95	Transmission Electron Microscopy Specimen Preparation for Two Dimensional Material Using Electron Beam Induced Deposition of a Protective Layer in the Focused Ion Beam Method. Applied Microscopy, 2018, 48, 122-125.	0.8	2
96	Method of Ga removal from a specimen on a microelectromechanical system-based chip for in-situ transmission electron microscopy. Applied Microscopy, 2020, 50, 22.	0.8	2
97	Self-Catalytic Growth of Elementary Semiconductor Nanowires with Controlled Morphology and Crystallographic Orientation. Nano Letters, 2021, 21, 9909-9915.	4.5	2
98	The role of a ternary Niâ€Snâ€P layer as a diffusion barrier in the Snâ€Ag solder/electroless Niâ€P system. Surface and Interface Analysis, 2012, 44, 1503-1506.	0.8	1
99	Effects of atmospheric pressure plasma surface treatments on the patternability and electrical property of screen-printed Ag nanopaste. Metals and Materials International, 2013, 19, 829-834.	1.8	1
100	Density Control and Wettability Enhancement by Functionalizing Carbon Nanotubes with Nickel Oxide in Aluminum-Carbon Nanotube System. Journal of Nanoscience and Nanotechnology, 2013, 13, 7685-7688.	0.9	1
101	Transmission Electron Microscopy Characterization of Thermomechanically Treated Al3Ti–(8, 10, 15)% Cr Intermetallics. Microscopy and Microanalysis, 2013, 19, 89-94.	0.2	1
102	Meso-Scale Transmission Electron Microscope Tomography Applied for Wax Distribution in Toner Particles. Microscopy and Microanalysis, 2013, 19, 58-61.	0.2	1
103	Grain Growth and Precipitation in Nanostructured 304SS After Heat Treatment. Journal of Nanoscience and Nanotechnology, 2017, 17, 7436-7441.	0.9	1
104	Electrical properties of the HfO <sub>2</sub> /Al <sub>2</sub> O <sub>3</sub> dielectrics stacked using single- and dual-temperature atomic-layer deposition processes on In <sub>0.53</sub> Ga <sub>0.47</sub> As. Semiconductor Science and Technology, 2019, 34, 105018.	1.0	1
105	Millimeter-Scale Growth of Single-Oriented Graphene on a Palladium Silicide Amorphous Film. ACS Nano, 2019, 13, 1127-1135.	7.3	1
106	Phase Change <i>via</i> Intermediary Metastable Local Structure of Ge Atoms in Ge <sub>2</sub> Sb <sub>2</sub> Te <sub>5</sub> Nanowires during Electrical Switching. ACS Applied Electronic Materials, 2020, 2, 2418-2428.	2.0	1
107	Quantification of the Nano-Voids in Electroless Deposited Copper Layers Using SiNx TEM Grids. Journal of the Electrochemical Society, 2021, 168, 102504.	1.3	1
108	Recrystallization Behavior of Shot Peened Pure Nickel Investigated by Backscattered Electron Techniques. Science of Advanced Materials, 2016, 8, 2103-2107.	0.1	1

#	Article	IF	CITATIONS
109	Quantification of Crystallinity in Ge–Sb–Te Chalcogenide Materials Using Energy-Filtered Electron Diffraction. Science of Advanced Materials, 2016, 8, 2276-2280.	0.1	1
110	Novel Method of Measuring the Thickness of Nanoscale Films Using Energy Dispersive Xâ€Ray Spectroscopy Line Scan Profiles. Advanced Materials Interfaces, 0, , 2101489.	1.9	1
111	<i>In Situ</i> Observation of the Early Stages of Rapid Solid–Liquid Reaction in Closed Liquid Cell TEM Using Graphene Encapsulation. Microscopy and Microanalysis, 2022, 28, 53-60.	0.2	1
112	Large-Scale Synthesis of High-Quality Double-Walled Carbon Nanotubes by Catalytic Decomposition of n-Hexane ChemInform, 2004, 35, no.	0.1	0
113	Evolution of Core-Shell Structure Using Functional Polystyrene and Gold. Molecular Crystals and Liquid Crystals, 2007, 472, 193/[583]-200/[590].	0.4	0
114	In situ observation of electron beam irradiation effects in oxidized polycrystalline Si1â^'xGex films. Thin Solid Films, 2008, 516, 3486-3492.	0.8	0
115	Fabrication of CdTe/Te Hetero-Nanostructures by Vapor-Solid Process. Journal of Nanoscience and Nanotechnology, 2011, 11, 6559-6562.	0.9	0
116	Mechanism of Pt Loading on Multi-Walled Carbon Nanotubes. Journal of Nanoscience and Nanotechnology, 2011, 11, 6293-6297.	0.9	0
117	Spatial Distribution of Dislocations in Relation to a Substructure in High-Quality GaN Film. Microscopy and Microanalysis, 2013, 19, 127-130.	0.2	0
118	B13-P-05In-situ scanning electron microscopy observation of electric field induced domain switching behavior in ferroelectric materials. Microscopy (Oxford, England), 2015, 64, i95.1-i95.	0.7	0
119	B22-P-05Observation of recrystallization behavior of shot-peened pure nickel using ECCI combined with EBSD. Microscopy (Oxford, England), 2015, 64, i105.1-i105.	0.7	0
120	<i>In situ</i> Measurement of the Adhesion Strength and Effective Elastic Stiffness of Single Soft Micropillar. Journal of Adhesion, 2015, 91, 369-380.	1.8	0
121	In Situ Transmission Electron Microscopy Study on the Reaction Kinetics of the Ni/Zr-interlayer/Ge System. Applied Microscopy, 2015, 45, 16-22.	0.8	0
122	Cross-Sectional Transmission Electron Microscopy Sample Preparation of Soldering Joint Using Ultramicrotomy. Applied Microscopy, 2016, 46, 167-169.	0.8	0
123	Microstructural Evolution and Recrystallization Behavior Traced by Electron Channeling Contrast Imaging. Applied Microscopy, 2018, 48, 130-131.	0.8	0
124	Grain Boundaries Imaged by Integration of Sobel Filtered Scanning Transmission Electron Micrographs. Applied Microscopy, 2018, 48, 132-133.	0.8	0